RSC Advances

PAPER

View Article Online
View Journal | View Issue

Cite this: *RSC Adv.*, 2017, **7**, 40131

Metabolic profiling of myrislignan by UPLC-ESI-QTOFMS-based metabolomics

Xiao-Nan Yang,†[a] Qian-Qian Lv,†[ab] Qi Zhao,[ac] Xin-Mei Li,[a] Dong-Mei Yan,*[d] Xiu-Wei Yang[e] and Fei Li *[a]

Myrislignan (MRL) is a bioactive 8-O-4′-neolignan distributed in nutmeg that is an official Traditional Chinese Medicine used for the treatment of gastrointestinal diseases in China. In the present study, the metabolic map of MRL was determined in mouse by ultra-performance chromatography electrospray ionization quadrupole time-of-flight mass spectrometry (UPLC-ESI-QTOFMS)-based metabolomics. A total of 23 MRL metabolites (19 were newly identified) were determined in both *in vivo* and *in vitro* metabolism of MRL. It was found that hydroxylation and demethylation were the major metabolic pathways for MRL metabolism *in vitro* and *in vivo*, respectively. Recombinant cytochrome P450s (CYPs) screening revealed that CYP3A4 and CYP3A5 played a crucial role in the metabolism of MRL. Interestingly, MRL and its metabolites were prone to generate the high abundance ions of Na^+ adducts due to one 8-O-4′ type bond in their molecular structures. Taken together, these data reveal the metabolic map of MRL, contributing to the understanding of the metabolism and disposition of 8-O-4′-neolignans in nutmeg.

Received 3rd June 2017
Accepted 2nd August 2017

DOI: 10.1039/c7ra06189g

rsc.li/rsc-advances

Introduction

Lignans are natural polyphenolic compounds found in plants, which are commonly derived from two molecules of phenylpropanoids *via* dimerization of monolignols to a dibenzylbutane skeleton. Generally, the plant lignans are two phenylpropanoid units linked by a bond connect to each central (8–8′) carbon atom of the side chain,[1] however, the two phenylpropanoid units are joined to other carbon atom in neolignans.[2] Studies revealed that lignans possess anticancer, antimicrobial, antiviral, anti-fungal and antiatherosclerotic effects.[3] Additionally, lignans can suppress lipid peroxidation and free radical-mediated process, and show antioxidant activity.[4]

Nutmeg is the dried seed of *Myristica fragrans* Houtt. which contains lignans and neolignans.[5] Nutmeg has been used as folk medicine for treatment of rheumatic disorders,[6] hyperglycaemia, hyperlipidaemia,[7] diarrhea,[8] flatulence[9] and toxoplasmosis[10] for a long time. Many lignan and neolignan compounds have been isolated and identified from nutmeg[11]. Myrislignan (MRL), *erythro*-(1*R*,2*S*)-2-(4-allyl-2,6-dimethoxyphenoxyl)-1-(4-hydroxy-3-methoxyphenyl)propan-1-ol, is a major and representative 8-O-4′-neolignan in nutmeg (Fig. 1). Studies have demonstrated the MRL may affect hepatic mixed function oxidase enzyme activity.[12] It also exhibits multiple biological activities, including the decrease of lipopolysaccharide-induced nitric oxide production,[13] inhibition of vascular smooth muscle contraction[14] and antifungal properties.[15] Using Caco-2 cell

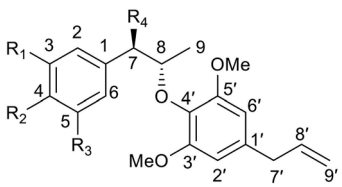

Compound	R1	R2	R3	R4
Myrislignan	OCH_3	OH	H	OH
Myrifralignan D	OCH_3	OH	OCH_3	OH
a	OCH_3	OCH_3	OCH_3	OH
b	OCH_3	OCH_3	H	OH
c	OCH_3	OCH_3	OCH_3	H

Fig. 1 Chemical structures of typical 8-O-4′-neolignans in nutmeg. (a) *erythro*-2-(4-Allyl-2,6-dimethoxyphenoxy)-1-(3,4,5-trimethoxyphenyl)propan-1-ol; (b) *erythro*-2-(4-allyl-2,6-dimethoxyphenoxy)-1-(3,4-dimethoxyphenyl)propan-1-ol; (c) *erythro*-2-(4-allyl-2,6-dimethoxyphenoxy)-1-(3,4,5-trimethoxyphenyl)propan.

[a]*State Key Laboratory of Phytochemistry and Plant Resources in West China, Kunming Institute of Botany, Chinese Academy of Sciences, Kunming 650201, China. E-mail: lifeib@mail.kib.ac.cn; Tel: +86-871-65216953*

[b]*Research Center for Differentiation and Development of Basic Theory of Traditional Chinese Medicine, Jiangxi University of Traditional Chinese Medicine, Nanchang 330004, China*

[c]*University of Chinese Academy of Sciences, Beijing 100049, China*

[d]*School of Pharmacy, Jiangxi University of Traditional Chinese Medicine, Nanchang 330004, China. E-mail: yanli1999@163.com; Tel: +86-791-87118995*

[e]*School of Pharmaceutical Sciences, Peking University Health Science Center, Peking University, Beijing 100191, China*

† These authors contributed equally to this work.

monolayer model revealed that 8-O-4′-neolignans have high permeability in the intestine.[16] Pharmacokinetics, distribution, and metabolism of MRL in the rats have been investigated.[17,18] Seven metabolites of MRL have been identified following the incubation with rat liver microsome.[19] There are limited studies to determine its *in vivo* metabolism and which cytochrome P450s (CYPs) are involved in MRL metabolism. Metabolic profiling of the major components is important to explain the efficacy of Traditional Chinese Medicine and predict its toxicity. Therefore, a more sensitive and efficient approach used to determine the metabolic map of MRL is required.

Ultra-performance chromatography electrospray ionization quadrupole time-of-flight mass spectrometry (UPLC-ESI-QTOFMS)-based metabolomics has been widely used for the comprehensive profiling of xenobiotic metabolism. Due to its high sensitivity and selectivity, the metabolic behaviors of many clinical drugs including procainamide,[20] gefitinib,[21] and noscapine[22] have been determined by UPLC-ESI-QTOFMS-based metabolomics, yielding new insights on their efficacy and side-effects. Using this powerful technology, the metabolic maps of many bioactive natural compounds have been described, such as arecoline[23] and osthole.[24] The aims of the present study were performed by metabolomics approach based on UPLC-ESI-QTOFMS, and (i) to identify the metabolites of MRL *in vivo* and *in vitro*; (ii) to determine the drug-metabolizing enzymes involved in MRL metabolism; (iii) to draw the metabolic map of MRL. These results reveal the metabolism and disposition of MRL following its exposure to the human and animal.

Experimental

Chemicals and reagents

MRL was purchased from Beta Biotechnology Co., Ltd (Nanchang, China). NADPH, chlorpropamide, and formic acid were obtained from Sigma-Aldrich (St. Louis, MO, USA). Mouse liver microsome (MLM) and human liver microsome (HLM) for *in vitro* metabolism were provided by Bioreclamationivt Inc. (Hicksville, NY, USA). Recombinant human CYPs were purchased from Xenotech, LLC (Kansas City, KS, USA). All other reagents were of analytical grade or chromatographically pure when appropriate.

Animal experiment and biological samples preparation

C57BL/6 mice (6–7 weeks, 20–22 g) were provided by Slaccas Laboratory Animal Co., LTD. (Hunan, China). The animals were acclimatized to the facilities for 1 week in a room at 23 ± 1 °C with a light/dark cycle of 12/12 h and humidity 50–60%. Sterile tap water and standard rodent chow were allowed *ad libitum*. Then the mice were randomly divided into two groups with four animals in each group. MRL was suspended in 0.5% sodium carboxymethylcellulose (CMC-Na). One group of animals was administered by intragastrically with 200 mg kg^{-1} of MRL, and another group of animals received 0.5% CMC-Na used as the control group. The animals were immediately put in metabolism cages individually after treatments. Urine and feces were collected for a period of 0–24 h. Samples were stored at −80 °C until analysis. Animals were maintained in accordance with the guidelines of the Chinese Academy of Sciences, Kunming, China, and approved by the institutional ethical committee (IEC) of Kunming Institute of Botany.

Samples preparation were carried out according to the report of Zhao, *et al.*[24] Urine samples were prepared by adding 20 μL of urine into 180 μL of 50% aqueous acetonitrile containing 5 μM of chlorpropamide as the internal standard. After vortexing for 1 min, the urine samples were centrifuged at 18 000*g* for 20 min to remove proteins and particulates. For feces samples, 20 mg of feces were homogenized with 10 fold of 50% aqueous acetonitrile, and shaken at room temperature for 20 min. The samples were centrifuged at 18 000*g* for 20 min. Subsequently, 100 μL of each supernatant from feces sample was transferred to a new Eppendorf tube and diluted with 200 μL of 50% aqueous acetonitrile containing 5 μM chlorpropamide. The diluted solutions were again centrifuged at 18 000*g* for 20 min. A 5 μL aliquot of each sample was injected for UPLC-ESI-QTOFMS analysis to identify the potential metabolites of MRL.

In vitro metabolism of MRL

The metabolism of MRL *in vitro* was conducted in 96 wells plate. Briefly, 180 μL of incubation system contained 50 mM of MRL, 0.5 g mL^{-1} of MLM or HLM or 2 pmol mL^{-1} of each c-DNA-expressed CYPs (control, CYP1A1, 1A2, 1B1, 2A6, 2B6, 2C19, 2C8, 2C9, 2D6, 2E1, 3A4, 3A5, and 4A11) was pre-incubated at 37 °C for 5 min. After that, the reaction was initiated by adding 20 μL of NADPH (10 mM) into the system. The absence of NADPH in system was incubated separately as vehicle control. Incubations were carried out at 37 °C and 800 rpm for 40 min in a MicBio II incubator (Abson). After incubation, each liquid was transferred to 1.5 mL centrifuge tube, and then reactions were completed by adding 200 μL of ice cold acetonitrile. The solution was followed by centrifuged at 18 000*g* for 20 min at 4 °C, and 5 μL aliquot of the supernatant was prepared for UPLC-ESI-QTOFMS injection. The incubations were conducted in triplicates.

UPLC-ESI-QTOFMS analysis

Chromatographic analysis was performed on an Agilent 1290 Series (Agilent, Santa Clara, CA, USA) UPLC system equipped with a 1290 Quat Pump, a thermostatically controlled column apartment and an auto plate sampler. MRL and its metabolites were separated by an XDB-C18 column (2.1 × 100 mm, 1.8 μm, Agilent, Santa Clara, CA, USA) at 45 °C. The mobile phase consisted of A, 0.01% of formic acid in water and B, 0.01% of formic acid in acetonitrile. Gradient elution of 2–98% B from 0 to 12 min, 98% B from 12 to 14 min and 2% B from 14 to 16 min was used for metabolites separation. Data were collected in positive mode by the electrospray ionization 6530 QTOFMS (Agilent, Santa Clara, CA, USA). Nitrogen was used as collision gas and drying gas (9 L min^{-1}) which was set at 350 °C. The nebulizer pressure was kept at 35 psi, and 3.5 kV was set for capillary voltage. Chlorpropamide (5 μM) was used as the internal standard.

Identification of xenobiotic metabolites

The identification and confirmation of xenobiotic metabolites (MRL metabolites) were performed according the previous descriptions.[20,22] The xenobiotic metabolites were presumed and preliminary determined by OPLS-DA analysis. Tandem MS of selected metabolites was carried out in the targeted mode by collision energy of 20 eV. The chemical structures of MRL metabolites were deduced based on their MS/MS fragmentation patterns. Mass error based on the elemental compositions of each metabolite was calculated by Seven Golden Rules.[25]

Data analysis

Chromatographic and spectral data were acquired by Mass-Hunter Workstation data Acquisition software (Agilent, Santa Clara, CA, USA). Mass Profiler Professional software (Agilent, Santa Clara, CA, USA) was used for data alignment, and to generate a data matrix containing peak areas corresponding to a sample ID, unique *m*/*z* and retention time. Then the generated data matrix was further introduced to SIMCA-P+13.0 software (Umetrics, Kinnelon, NJ, USA) for principal component analysis (PCA) and orthogonal projection to latent structures-discriminant analysis (OPLS-DA). Potential metabolites of MRL were initially identified by analyzing the ions contributing to the separation from control group in the S-plot of OPLS-DA. *In vivo* analysis, the relative abundance was evaluated based on the peak areas of ion counts and normalized by the peak area of internal standard. *In vitro* analysis, the sum of peak areas of total detected ion counts was integrated as 100%. The values of experiments were presented as mean ± SEM. Statistical analysis was performed by using Prism v. 6 (GraphPad Software, San Diego, CA, USA).

Results

Metabolomics profiling of MRL metabolites *in vivo* and *in vitro*

The *in vivo* metabolism of MRL was conducted in C57BL/6 mice. Due to the weak signal of MRL in ESI^- mode, the metabolites in urine and feces of MRL were analyzed by UPLC-ESI-QTOFMS in the full scan ESI^+ mode. The MRL treatment group was well separated from vehicle group by both PCA and OPLS-DA models (Fig. 2A and B). To better determine the metabolites of MRL, the loadings scatter S-plot was conducted to the separation of exogenous metabolites in urine samples (Fig. 2C).

Total four phase I metabolites of MRL were determine from urine sample including **M6**, **M9**, **M10** and **M11**, and parent MRL also existed in urine. Eleven phase II metabolites of MRL (**M13–M23**) were detected in urine sample. Most of these metabolites were the glucuronide adducts of phase I metabolites (**M13–M22**), and **M23** was a sulfated product of parent MRL (Fig. 3A). Only three metabolites (**M9**, **M10** and **M11**) with parent MRL were found from feces sample (Fig. 3A). All of these metabolites were identified as the new metabolites of MRL. Combined the metabolites generated from the same type of metabolic reaction, demethylation was found to be the major metabolic reaction of MRL revealed by the total relative abundance of demethylated metabolites and demethylation followed by glucuronidated metabolites was the highest (Fig. 3B). The observed *m*/*z* coupled with major fragment ions, retention time, mass error, molecular formula and the source of the metabolites are listed in Table 1.

To clarify the metabolic pathway and predict the metabolic differences between human and mouse, the phase I metabolisms of MRL were performed in mouse liver microsome (MLM) and human liver microsome (HLM) incubation systems. The MRL treatment and control group could be well separated from each other by PCA model (Fig. 4A), and the potential metabolites were primarily determined from S-plot (Fig. 4B). The phase I metabolites of MRL were further separated from endogenous metabolites by the trend plots which was generated from S-plot (example of Fig. 4C and D). Overall, twelve MRL metabolites (**M1–M12**) were identified in MLM incubation system (Table 1). Among these metabolites, **M1**, **M3**, **M4** and **M7** have been reported in the previous study.[19] The structures of other eight metabolites (**M2**, **M5**, **M6**, and **M8–M12**) were found in this study and determined as novel MRL metabolites. The metabolites of MRL in HLM incubation system were similar to that in the MLM incubation system (Table 1). The percentage of whole detected metabolites of MRL is shown in Fig. 5A. The percentage of parent MRL was 71.16% in MLM and 42.73% in HLM, indicating that mice liver microsome shows lower metabolic rate than human liver microsome.

In MLM incubation system, the hydroxylated metabolites of MRL presented as the major metabolites (16.45% of total identified metabolites) and followed by demethylated metabolites (6.08% of total identified metabolites). In HLM incubation system, the hydroxylated metabolites of MRL were the highest among all the identified metabolites (Fig. 5B). This result demonstrated that hydroxylation is a crucial metabolic pathway for MRL in both MLM and HLM metabolism.

Identification and structural elucidation of phase I metabolites of MRL

PCA analysis initially suggested some potential phase I metabolites of MRL. The chemical structures of these metabolites were further identified by the accurate mass measurement and tandem MS fragmentography. Positive ion mode ESI mass spectra were used to collect data. The precursor ions $[M + Na]^+$ of these metabolites were selected and subsequently fragmented in MS/MS mode to obtain product ions spectra and yield useful structural information. The observed *m*/*z* of MS/MS fragments ions are shown in Table 1.

MRL was calculated as $C_{21}H_{26}O_6$ based on the accurate mass measurement $[M + Na]^+$ ion (*m*/*z* 397.1623^+), and the main MS/MS fragmentation ions of MRL were 326, 283, 216, 173 and 108. The *m*/*z* 216 had the highest response in the secondary mass spectrometry, which was eliminated the group of $C_7H_7O_2$, CH_3O, and C_2H_3.

Metabolite **M1** was calculated as $C_{14}H_{20}O_4$ based on the accurate mass measurement $[M + Na]^+$ ion (*m*/*z* 275.1258^+). Compared with the $[M + Na]^+$ ion (*m*/*z* 397.1643^+) of parent MRL, **M1** was 122 Da ($C_7H_6O_2$) lower than MRL. In addition, the *m*/*z*

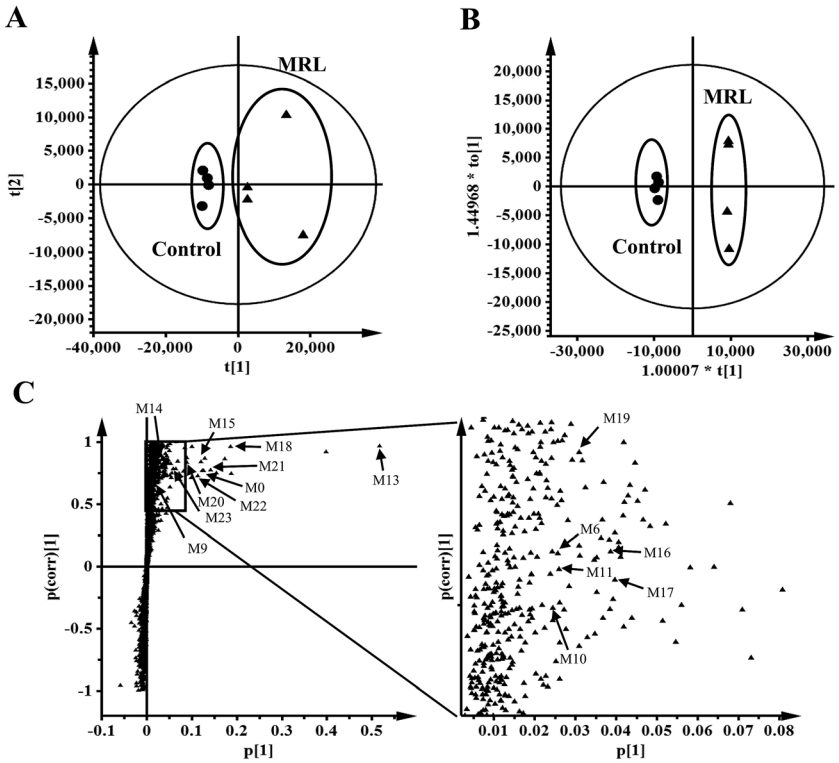

Fig. 2 Metabolomics analysis of MRL metabolites in mouse urine. (A) Scores scatter plot of PCA model to characterize control group of mice (without MRL) and MRL-treated mice (200 mg kg^{-1}). (B) Analysis of control and MRL-treated mice urine by OPLS-DA score plots (●, vehicle-treated mice in score plots; ▲, MRL-treated mice in score plots). (C) OPLS loading S-plot. In PCA scores plot, the *t*[1] and *t*[2] correspond to principal components 1 and 2, respectively. In the OPLS-DA scores plot, the *t*[1] and to[1] values represent the score of each sample in principal component 1 and 2. The *p*(corr)[1] and *p*[1] values in S-plot represent the interclass difference and the relevant abundance of ions, respectively. Metabolites are labeled in S-plot.

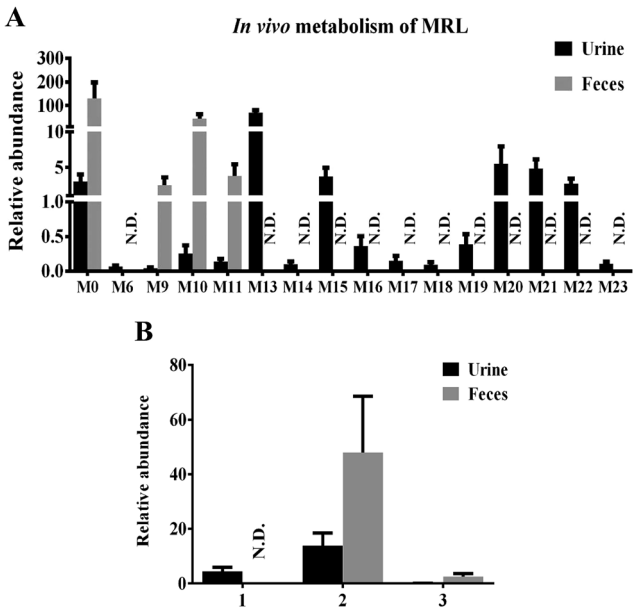

Fig. 3 Excretion of MRL metabolites in mouse urine and feces. (A) Contents of MRL metabolites in mouse urine and feces. (B) Comparison of the major metabolic pathway *in vivo*. Reaction types: (1) hydroxylation and hydroxylation followed by glucuronidation; (2) demethylation and demethylation followed by glucuronidation; (3) oxidation. N.D., not detected. Data were presented as mean ± SEM.

216 fragment ion by **M1** is consistent with the main fragment ion of MRL. **M1** is a metabolite obtained by decomposing the left benzene ring fraction ($C_7H_6O_2$) of MRL.

The excimer ions of **M2**, **M3** and **M4** were *m*/*z* 291 ($[M + Na]^+$), which were 16 Da larger than **M1**. Neutral losses of 28 (C_2H_4) suggested the existence of vinyl group in metabolites **M2** and **M3**, and **M3** subsequently neutral losses of 28 (CO) fragment ion, suggested that its structure contains 1-hydroxyallyl. **M4** was eliminated the group of C_2H_4O, and speculated that its structure contains 3-hydroxy-prop-1-enyl. According to above reasoning, **M2**, **M3** and **M4** were the hydroxylation products of **M1**, and their hydroxylation occurs on the benzene ring, position C7′ and C9′, respectively. The tandem MS spectra and fragmentation pattern of **M2** was shown in Fig. 6A.

Metabolites **M5**, **M6**, **M7** and **M8** were calculated as $C_{21}H_{26}O_7$ based on their excimer ions ($[M + Na]^+$), and higher by 16 Da (O) than MRL, indicating that they were the hydroxylation products of MRL. The product ions at *m*/*z* 232 of **M5**, **M6** and **M7** were higher by 16 Da than the product ion of MRL at *m*/*z* 216, suggesting that **M6**, **M7** and **M5** may be the hydroxylation products of MRL on C9, C7′ and benzene ring on the C2′ or C6′ position. **M5** was eliminated the groups of CH_3 and C_3H_6, thus indicating that **M5** was hydroxylation metabolite on the benzene ring of MRL. The elimination of the group of 27 (C_2H_3) suggested the existence of vinyl group in metabolites **M6** and **M7**, and **M7** also

Table 1 Summary of metabolites of MRL produced *in vivo* and *in vitro* metabolism

Metabolites (ID)	R_t (min)	Observed *m/z* $[M + Na]^+$	Major fragment ions (*m/z*)	Mass error (ppm)	Molecular formula	Source
M0	9.7	397.1623	326, 283, 216, 173	0.35	$C_{21}H_{26}O_6$	MLM, HLM, urine, feces
M1	8.9	275.1258	216, 176	−1.53	$C_{14}H_{20}O_4$	MLM, HLM
M2[a]	6.2	291.1203	242, 232, 215, 199	0.03	$C_{14}H_{20}O_5$	MLM, HLM
M3	6.8	291.1198	245, 231, 181, 153	−1.68	$C_{14}H_{20}O_5$	MLM, HLM
M4	7.7	291.1202	273, 251, 216, 194	−0.31	$C_{14}H_{20}O_5$	MLM, HLM
M5[a]	7.1	413.1569	381, 339, 308, 232	−0.41	$C_{21}H_{26}O_7$	MLM, HLM
M6[a]	7.3	413.1571	396, 337, 277, 232, 215	0.07	$C_{21}H_{26}O_7$	MLM, HLM, urine
M7	7.9	413.1577	324, 232, 204	1.52	$C_{21}H_{26}O_7$	MLM, HLM
M8[a]	8.7	413.1571	384, 302, 216	0.07	$C_{21}H_{26}O_7$	MLM, HLM
M9[a]	8.6	289.1048	251, 229, 204	0.56	$C_{14}H_{18}O_5$	MLM, HLM, urine, feces
M10[a]	8.8	383.1450	325, 261, 216	−3.94	$C_{20}H_{24}O_6$	MLM, HLM, urine
M11[a]	9.0	383.1468	365, 323, 277, 229, 202	0.72	$C_{20}H_{24}O_6$	MLM, HLM, urine, feces
M12[a]	8.2	261.1110	202, 168	4.87	$C_{13}H_{18}O_4$	MLM, HLM
M13[a]	7.5	573.1925	397, 379, 216	−3.05	$C_{27}H_{34}O_{12}$	Urine
M14[a]	6.8	451.1582	275, 216,	7.76	$C_{20}H_{28}O_{10}$	Urine
M15[a]	5.7	589.1881	413, 381, 232	−1.80	$C_{27}H_{34}O_{13}$	Urine
M16[a]	6.0	589.1901	413, 396, 307, 232, 215	1.60	$C_{27}H_{34}O_{13}$	Urine
M17[a]	6.9	589.1866	413, 370, 317, 232	−4.34	$C_{27}H_{34}O_{13}$	Urine
M18[a]	7.2	589.1877	413, 391, 362, 216	−2.48	$C_{27}H_{34}O_{13}$	Urine
M19[a]	6.3	559.1771	383, 216	−1.61	$C_{26}H_{32}O_{12}$	Urine
M20[a]	7.3	559.1776	383, 216	−1.79	$C_{26}H_{32}O_{12}$	Urine
M21[a]	6.6	559.1773	383, 202	−2.32	$C_{26}H_{32}O_{12}$	Urine
M22[a]	7.1	559.1780	383, 202	−1.07	$C_{26}H_{32}O_{12}$	Urine
M23[a]	8.4	477.1186	397, 379	−0.07	$C_{21}H_{26}SO_9$	Urine

[a] Indicate novel metabolites found in this study.

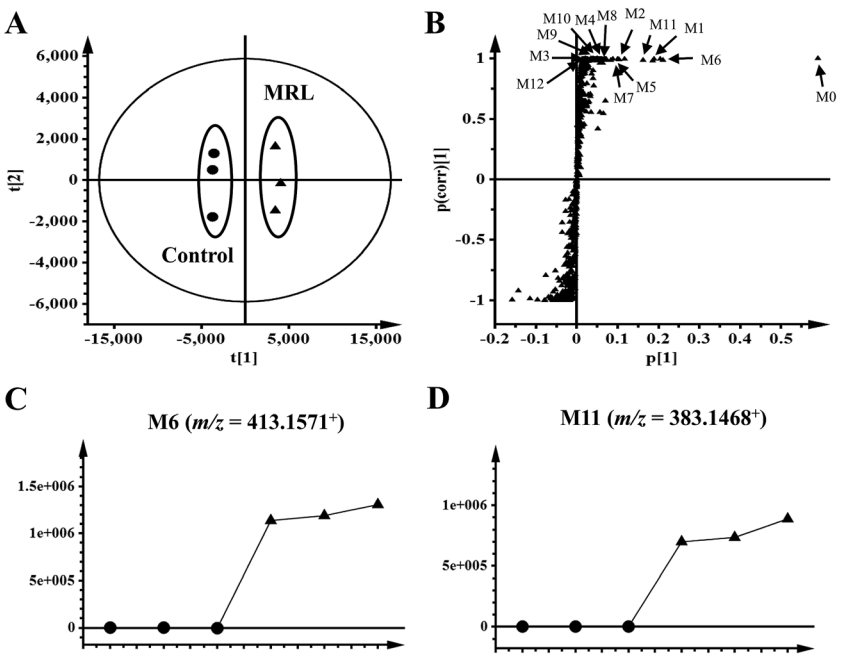

Fig. 4 Metabolomics analysis of MRL metabolites in mouse liver microsome. (A) Scores plot of an OPLS-DA model from MLM incubation mixture without drug (control) and with MRL. (B) OPLS-DA loading S-plot. (C) Trend plot of **M6** in MLM with and without MRL. (D) Trend plot of **M11** in MLM with and without MRL. (●, control-treated MLM; ▲, MRL-treated MLM). Metabolite codes correspond to those in Table 1.

neutral losses of 28 (CO) fragment ion, suggested that its structure contains 1-hydroxyallyl. Therefore, **M6** and **M7** were determined as C9-hydroxyl and C7′-hydroxyl metabolites of MRL. The elimination of the group of 29 (CHO) suggested the existence of aldehyde group in metabolite **M8**, and the *m/z* 216 fragment ion by **M8** was consistent with the main fragment ion of MRL, suggesting that **M8** was the C9′-hydroxylation and rearrangement

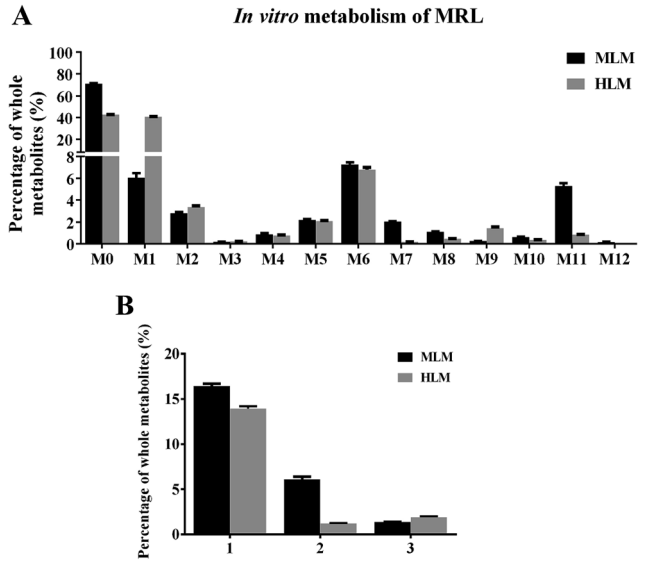

Fig. 5 *In vitro* metabolisms of MRL by liver microsomes. (A) Metabolites of MRL in mouse liver microsome (MLM) and human liver microsome (HLM) incubation systems. (B) Comparison of the major metabolic pathway *in vitro*. Reaction types: (1) hydroxylation; (2) demethylation; (3) oxidation. Data were presented as mean ± SEM.

product of MRL. The tandem MS spectra and fragmentation pattern of **M6** and **M8** were shown in Fig. 6B and C.

Metabolite **M9** was deduced as $C_{14}H_{18}O_5$ based on the accurate mass measurement $[M + Na]^+$ ion (m/z 289.1048$^+$), and was 2 Da (H_2) lower than **M4**. The elimination of the group of 29 (CHO) suggested the existence of aldehyde group in metabolite **M9**, indicating that **M9** was the oxidation product of **M4**.

The elimination of the group of 27 (C_2H_3) or 28 (C_2H_4) suggested the existence of vinyl group in metabolites **M10**, **M11** and **M12**. Metabolites **M10** and **M11** were calculated as $C_{20}H_{24}O_6$ based on the accurate mass of $[M + Na]^+$ ions (m/z 383.1451$^+$ and m/z 383.1468$^+$), and both lower by 14 Da (CH_2) than MRL. Additionally, the product ion at m/z 216 of **M10** was the same as the product ion found in MRL and the product ion at m/z 202 of **M11** was lower by 14 Da than the product ion of MRL at m/z 216, indicating that **M10** was the C3–*O*-demethylation metabolite of MRL and **M11** was the C3′-demethylation or C5′-demethylation metabolite of MRL. Metabolite **M12** was deduced as $C_{13}H_{18}O_4$ based on the accurate mass of $[M + Na]^+$ ion (m/z 261.1110$^+$), and lower by 14 Da (CH_2) than **M1**, and the product ion at m/z 202 of **M12** was lower by 14 Da than the product ion of **M1** at m/z 216, suggesting that **M12** was the demethylation product of **M1**. The tandem MS spectra and fragmentation pattern of **M11** was shown in Fig. 6D.

Identification of phase II metabolites of MRL

Metabolite **M13** was deduced as $C_{27}H_{34}O_{12}$ based on the accurate mass of $[M + Na]^+$ ion (m/z 573.1925$^+$), and was 176 Da ($C_6H_8O_6$) higher than MRL. The product ions at m/z 397 and 216 of **M13** were similar to the product ions found in MRL (Table 1), indicating that **M13** was glucuronic acid-conjugated product of

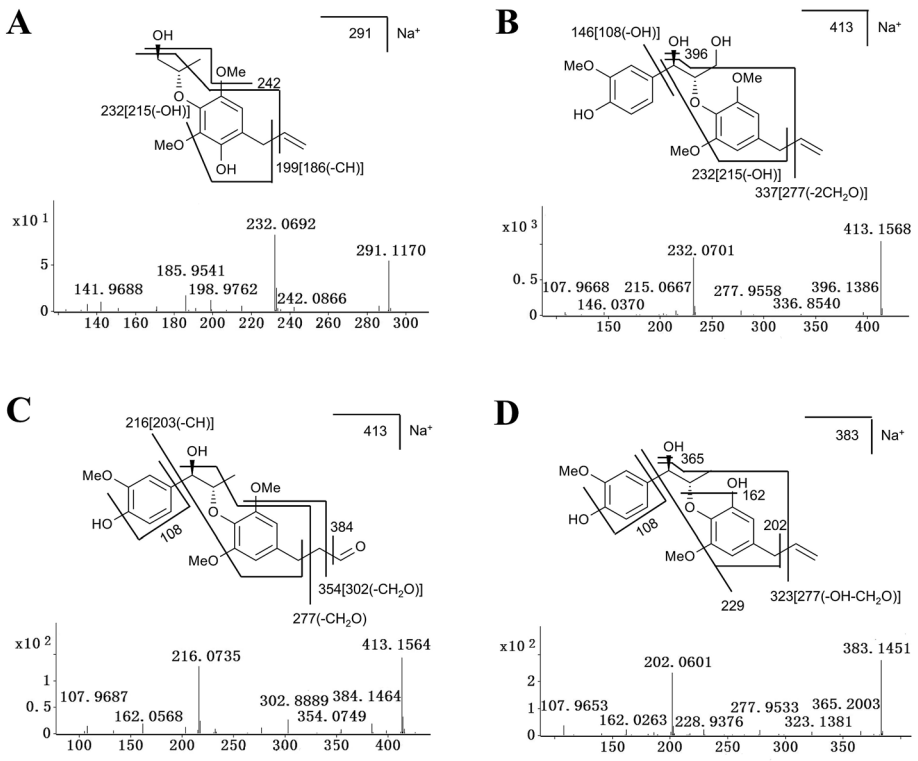

Fig. 6 Tandem MS spectra and fragmentation pattern of some representative metabolites of MRL. (A) Tandem MS spectra and chemical structure of **M2**. (B) Tandem MS spectra and chemical structure of **M6**. (C) Tandem MS spectra and chemical structure of **M8**. (D) Tandem MS and chemical structure of **M11**. MS/MS fragmentation was conducted with collision energy at 20 eV.

MRL. After elimination of the glucuronic acid group ($C_6H_8O_6$), metabolites **M14**, **M15**, **M16**, **M17**, and **M18** yielded fragment ions at *m*/*z* 275, 413, 413, 413 and 413 that were similar to the mass of **M1**, **M5**, **M6**, **M7** and **M8**, respectively. Therefore, metabolites **M14–M18** were glucuronic acid-conjugated products derived from **M1**, **M5**, **M6**, **M7** and **M8**, respectively. Metabolites **M19**, **M20**, **M21** and **M22** were calculated as $C_{26}H_{32}O_{12}$ based on their excimer ions ($[M + Na]^+$). **M19** and **M20** were eliminated the group of glucuronic acid ($C_6H_8O_6$), and the product ions at *m*/*z* 383 and 216 were similar to the product ions found in **M10**, indicating that **M19** and **M20** were glucuronic acid-conjugated product of **M10**. Similarly, **M21** and **M22** were eliminated the group of glucuronic acid ($C_6H_8O_6$), and the product ions at *m*/*z* 383 and 202 were similar to the product ions found in **M11**, indicating that **M21** and **M22** were glucuronic acid-conjugated product of **M11**. Metabolite **M23** was deduced as $C_{21}H_{26}SO_9$ based on the accurate mass of $[M + Na]^+$ ion (m/z 477.1186$^+$), and was 80 Da (SO_3) higher than MRL. The product ions at *m*/*z* 397 and 216 of **M23** were similar to the product ions found in MRL, indicating that **M23** was sulfuric acid-conjugated product of MRL.

Screening the CYPs involved in the metabolism of MRL

To date, there is no study reported which CYPs are involved in the metabolism of MRL. To verify the phase I enzymes involved in the metabolism, MRL was incubated with a panel of recombinant human P450s including CYP1A1, 1A2, 1B1, 2A6, 2B6, 2C19, 2C8, 2C9, 2D6, 2E1 3A4, 3A and 4A11. Among them, CYP3A4 and 3A5 were the most active enzymes of all the P450s for MRL metabolism (Table 2). The secondary enzymes for MRL metabolizing were CYP1A1 and 1A2 evidenced by CYP1A1 contributed to nine metabolites (**M1**, **M2**, **M4–M8**, **M10** and **M11**) generation and CYP1A2 corresponded to eight metabolites (**M1**, **M2**, **M5–M8**, **M10** and **M11**) of MRL, respectively. All recombined human CYPs were responsible for the formation of monohydroxylated MRL metabolites **M5** and **M6**. Among them, CYP1A1 and 2C19 exhibited highest catalytic activities towards the formation of **M6**, while CYP2C19 acted the key role in **M5** formation. Another monohydroxylated metabolite **M7** was produced by CYP2C8 mostly. CYP3A4 and 3A5 were the primary enzymes that cleaved parent MRL and formed metabolite **M1** followed by hydroxylation. Through this pathway, **M2**, **M3** and **M4** were mainly produced by CYP3A4/5. The demethylated metabolite **M10** was mainly transformed by CYP1A1, 3A5 and 1A2, and **M11** was mainly transformed by CYP2C9 and 1A2.

Discussion

MRL shows various biological activities and preliminary *in vitro* metabolism of MRL has been investigated,[19] however, the systematic *in vivo* metabolism of this compound and the CYPs involved in its metabolism are still not clear. The present study was aimed to decipher the metabolic map of MRL using metabolomics approach. By using this strategy, a series of hydroxylation, hydrogenation, demethylation, oxidation, glucuronidation, and sulfation metabolites of MRL were determined *in vivo* and *in vitro*. Combined with OPLS analysis, total fifteen metabolites (**M6**, **M9–M11**, **M13–M23**) were determined in mouse urine samples and three (**M9**, **M10** and **M11**) of them were found in feces samples. Parent MRL was also found in both of feces and urine samples and it was the most abundant metabolite in feces. The structures of these metabolites were further identified by MS/MS fragmentography. All of these phase II metabolites were novel metabolites of MRL. The main metabolic pathway *in vivo* was demethylation followed by glucuronidation ($-CH_3 + C_6H_8O_6$), and all of these glucuronidated metabolites were excreted in urine but not in feces. The secondary *in vivo* metabolic pathway was hydroxylation plus glucuronidation, and these metabolites were also mainly excreted in urine but not in feces. In the phase II metabolism, some charged species such as glutamine, glycine, sulfate, or glucuronic acid could be conjugated with the metabolites of xenobiotics.[26] The addition of these groups produces more

Table 2 Roles of CYP450s in the formation of MRL metabolites[a]

No.	Enzyme	M1	M2	M3	M4	M5	M6	M7	M8	M9	M10	M11	M12
0	Control	0.11	—	—	—	1.36	0.12	—	—	—	—	—	—
1	CYP1A1R	3.67	7.60	—	9.39	6.11	32.73	3.89	18.37	—	32.20	6.34	—
2	CYP1A2R	1.01	5.39	—	—	2.44	1.68	1.09	19.87	—	15.07	36.52	—
3	CYP1B1R	0.35	—	—	—	1.58	0.32	0.22	—	—	0.46	—	—
4	CYP2A6R	0.09	—	—	—	1.54	0.13	—	—	—	—	—	—
5	CYP2B6R	0.16	—	—	—	1.55	0.19	1.06	—	—	—	—	—
6	CYP2C19R	0.45	—	—	—	51.36	24.36	8.94	—	—	4.26	—	—
7	CYP2C8R	1.01	—	—	—	2.41	6.51	53.90	—	—	1.01	4.20	—
8	CYP2C9R	0.05	—	—	—	14.83	5.05	6.57	—	—	1.31	45.73	—
9	CYP2D6R	0.29	—	—	—	3.68	8.08	10.17	—	—	1.62	—	—
10	CYP2E1R	0.11	—	—	—	1.57	0.19	—	—	—	—	—	—
11	CYP3A4R	41.81	30.68	46.95	52.98	2.04	4.81	4.26	15.95	—	12.70	1.73	—
12	CYP3A5R	50.76	56.32	53.05	37.63	7.81	15.69	9.90	45.81	—	31.37	5.48	—
13	CYP4A11R	0.13	—	—	—	1.73	0.13	—	—	—	—	—	—

[a] cDNA-expressed CYPs (control, CYP1A1, 1A2, 1B1, 2A6, 2B6, 2C19, 2C8, 2C9, 2D6, 2E1, 3A4, 3A5, and 4A11) were used to examine the roles of in individual CYPs in MRL metabolism. All samples were analyzed by UPLC-ESI-QTOFMS. The total peak areas of each metabolite of MRL from all the CYPs were set as 100%. All data are expressed as mean ($n = 3$).

polar metabolites and increases the hydrophilicity of the metabolites of xenobiotics. Previous study has revealed that the level of phase I metabolites obviously increased in urine of rats, human and rabbits after the catalyzing of β-glucuronidase.[27] In this study, most of the phase II metabolites, including eleven corresponding glucuronides of phase I metabolites were discovered in urines of C57/BL6 mice (Fig. 3A). Among them, **M13** (glucuronidation of parent MRL) shows the highest abundance in urine. However, the parent MRL was excreted as the highest abundance in feces. The results indicate that MRL could be excreted through both urine and feces in which hydrophilic glucuronidated products are mainly excreted in urine and the hydrophobic phase I metabolites are mainly excreted through feces.

Drug metabolism is a complex process and plays essential role in determining the efficiency and safety of drugs.[28] Numerous metabolites were produced following the phase I metabolism and part of them are inactive substances which may lead to significant decrease of therapeutic potential of drugs. On the other hand, some active metabolites formed by phase I metabolic enzymes could induce adverse effects. Thus, systematically determination of the metabolic map of drugs is required. To elucidate the metabolic pathway of MRL *in vivo*, MLM and HLM was incubated with MRL, respectively. In this study, total twelve phase I metabolites were identified by MLM metabolism. The cleavage of left aromatic ring (1, 7 C–C bond broken) of MRL (Fig. 7) leading to the formation of **M1** was discovered, which is consistent with the previous report.[19] Furthermore, other phase I metabolites from **M1** were identified, including the hydroxylation at position C2′ of the aromatic ring leading to the generation of **M2**, the hydroxylation at position C7′ leading to the formation of **M3**, the hydroxylation

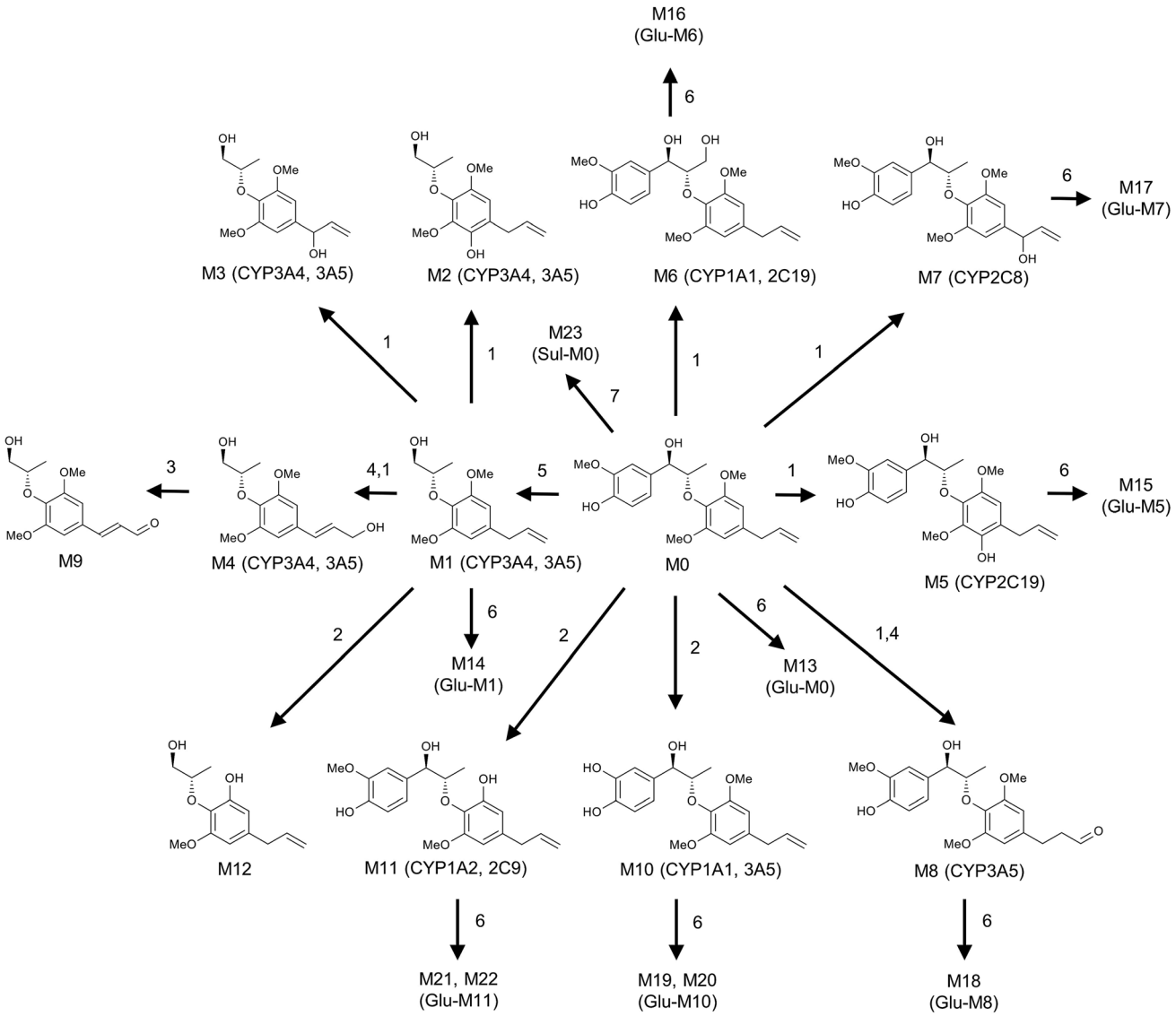

Fig. 7 Metabolic map of MRL. All structures of these metabolites were determined based on the exact mass measurement (mass error less than 10 ppm) and MS/MS fragments. Reaction types: (1) hydroxylation; (2) demethylation; (3) oxidation; (4) rearrangement; (5) decomposing; (6) glucuronidation; (7) sulfation.

of position C9′ subsequently to rearrangement of allyl group leading to the generation of **M4**, oxidation of 9′-OH group of **M4** resulting in the formation of **M9**, and cleavage of methyl group (position C5′-O) leading to the generation of **M12**. Using the present strategy, several phase I metabolites were newly identified. **M6**, the most abundant phase I metabolite of MRL was identified as hydroxylation at position C9 of the side chain (Fig. 6B). The hydroxylated metabolites **M5** and **M8**, and demethylated metabolites **M10** and **M11** were also identified. To compare MRL metabolism in human and mice, HLM metabolic system incubated with MRL was also performed in this study. As shown in Fig. 5A, the metabolites of HLM were similar to MLM. The relative contents of **M1** and **M9** from HLM metabolism were significantly higher than that of MLM, conversely, the percentage of **M7**, **M8** and **M11** were significantly lower than that of MLM metabolism. These data suggest that human and mice liver P450s shows the metabolic differences for MRL metabolism.

It was found that hydroxylation was the major phase I metabolic reaction in both mouse and human liver microsomes (Fig. 5B), followed by demethylation and oxidation. Recent years, human recombined cytochrome P450 enzymes (CYP450s) were used *in vitro* metabolism to discover the isoenzyme responsible for the metabolism of drugs.[29,30] To determine the role of individual CYP450 in MRL metabolism, parent MRL was incubated with a panel of recombinant human P450s including CYP1A1, 1A2, 1B1, 2A6, 2B6, 2C19, 2C8, 2C9, 2D6, 2E1 3A4, 3A and 4A11. CYP3A4 and 3A5 played the crucial roles in MRL metabolism evidenced by they involved in generation of most metabolites (Table 2). CYP3A4 and 3A5 is responsible for the metabolism of more than 50% of current drugs on the market and dietary polyphenols.[31] Qin *et al.* (2014) reported that lignans in WZ were the substrate of CYP3A, and the lignans competitive bound with CYP3A lead to increasing the plasma concentration of tacrolimus.[32] The high activities of CYP3A4 and 3A5 towards MRL biotransformation indicated that MRL may be the substrate of CYP3A4 and 3A5. Furthermore, the major metabolite **M6** was mainly produced by CYP1A1 and 2C19 (32.73 and 24.36%, respectively), and the high abundant metabolite **M11** was mainly formed by CYP1A2 and 2C9. The CYP2C19 is also an important drug metabolic enzyme.[33] The present study clarifies the subtype of CYPs involved in the metabolism of MRL.

Interestingly, MRL and its metabolites were prone to generate the high abundance ions of Na^+ adducts due to one 8-O-4′ type bond in the molecular structure. In addition, most of the daughter ions of these $[M + Na]^+$ were also observed as Na^+ adducts. Previous study shown that MRL could form a stable adduct ion ($[M + Na]^+$) in positive full-scan mode, nevertheless, it could not form the distinct product ions in MS/MS mode by using triple quadrupole mass spectrometer because in this mode, the energy is not enough to obtain fragments.[18] It was reported that Phillyrin that contains the ether bond in its molecular structure gave high abundance Na^+ adducts of parent ions and its fragment ions in positive MS/MS mode.[34] The MS/MS fragmentations of phillyrin were generated in ESI^+ mode when collision energy was set at 27 eV. The ether bond compounds 3-hydroxybutylphthalide-3-O-β-D-glucuronide and 3-hydroxybutylphthalide-3-*S*-acetylcysteine from Danggui Buxue Tang also could produce high abundance Na^+ adducts.[35] In our experiment, the signals of MRL and its metabolites in the ESI^- mode were extremely weak. The tandem MS of selected metabolites was preliminary conducted in the targeted mode by ramping collision energies from 5 to 25 eV in positive ESI mode. The appropriate collision energy was finally set at 20 eV because the daughter fragment ions of MRL metabolites could not be obtained below 20 eV, and the parent ions of MRL metabolites could not be detected when the collision energy was higher than 20 eV. Therefore, the relative high concentration of compounds and appropriate energy voltage of bombardment are essential for the generation of ions fragmentation of MRL metabolites.

Conclusion

In summary, the metabolism of MRL was investigated by UPLC-ESI-QTOFMS-based metabolomics in mouse model and liver microsomal incubation system. Total 23 MRL metabolites were identified *in vivo* and *in vitro* metabolism, including 19 newly identified metabolites. The comprehensive metabolic pathway of MRL was described (Fig. 7). Hydroxylation and demethylation were the major metabolic pathways for MRL metabolism *in vitro* and *in vivo*, respectively. The P450 enzymes involved in MRL metabolism were determined by recombinant cytochrome CYPs screening. CYP3A4 and 3A5 are found to be the major enzymes responsible for MRL metabolism. Our findings provide important information for the metabolism and disposition of 8-O-4′-neolignans in nutmeg. These results are essential for understanding MRL metabolism in mice, and provide fundamental for the investigation of MRL metabolism in humans.

Conflicts of interest

The authors have declared no conflict of interest.

Acknowledgements

This work was supported by the Thousand Young Talents Program of China, National Natural Science Foundation of China (81360509), State Key Laboratory of Phytochemistry and Plant Resources in West China (52Y67A9211Z1) and Post-doctoral targeted funding, Ministry of Human Resources and Social Security of Yunnan Province, China (39Y732921261).

References

1 R. S. Ward, *Chem. Soc. Rev.*, 1982, **11**, 75–125.
2 G. P. Moss, *Pure Appl. Chem.*, 2000, **72**, 1493–1523.
3 W. D. MacRae and G. N. Towers, *Phytochem. Rev.*, 1984, **23**, 1207–1220.
4 J. L. Ríos, R. M. Giner and J. M. Prieto, *Stud. Nat. Prod. Chem.*, 2002, **26**, 183–292.
5 X. W. Yang, X. Huang and M. Ahmat, *China J. Chin. Mater. Med.*, 2008, **33**, 397–402.
6 M. Adams, C. Berset, M. Kessler and M. Hamburger, *J. Ethnopharmacol.*, 2009, **121**, 343–359.

7 M. A. Kareem, S. G. Krushna, S. A. Hussain and K. L. Devi, *Trop. J. Pharm. Res.*, 2009, **8**, 337–344.
8 H. Kim, Y. Bu, B. J. Lee, J. Bae, S. Park, J. Kim, K. Lee, J. M. Cha, B. Ryu, S. J. Ko, G. Han, B. Min and J. W. Park, *J. Med. Food*, 2013, **16**, 953–956.
9 S. Chatterjee, Z. Niaz, S. Gautam, S. Adhikari, P. S. Variyar and A. Sharma, *Food Chem.*, 2007, **101**, 515–523.
10 S. Pillai, R. Mahmud, W. C. Lee and S. Perumal, *APCBEE Proc.*, 2012, **2**, 92–96.
11 Y. Wang and X. W. Yang, *Mod. Chin. Med.*, 2008, **2**, 004.
12 K. H. Shin and W. S. Woo, *Korean Biochem. J.*, 1990, **23**, 122–127.
13 G. Y. Cao, W. Xu, X. W. Yang, F. J. Gonzalez and F. Li, *Food Chem.*, 2015, **173**, 231–237.
14 K. Nakajima, T. Yamazaki, K. Kawashima, Y. Shinho, T. Kurashige, T. Nohara and M. Nishimura, Vascular smooth muscle contraction inhibitors from Myristica, JP 11080013, Jpn. Kokai Tokkyo Koho, 1999, p. 8.
15 M. Miyazawa, H. Kasahara and H. Kameoka, *Nat. Prod. Lett.*, 1996, **8**, 271–273.
16 X. W. Yang, X. Huang, L. Ma, Q. Wu and W. Xu, *Planta Med.*, 2010, **76**, 1587–1591.
17 Y. Wang, J.-X. Liu, Y.-B. Zhang, F. Li and X.-W. Yang, *Chromatographia*, 2012, **75**, 541–549.
18 Z. Zhu, S. Yang, W. Zhao, R. Li and C. Zhao, *J. Chromatogr. Sci.*, 2016, **54**, 689–696.
19 F. Li and X. W. Yang, *Phytochemistry*, 2008, **69**, 765–771.
20 F. Li, A. D. Patterson, K. W. Krausz, B. Dick, F. J. Frey, F. J. Gonzalez and J. R. Idle, *Biochem. Pharmacol.*, 2012, **83**, 1435–1444.
21 X. Liu, Y. Lu, X. Guan, B. Dong, H. Chavan, J. Wang, Y. Zhang, P. Krishnamurthy and F. Li, *Biochem. Pharmacol.*, 2015, **97**, 111–121.
22 Z. Z. Fang, K. W. Krausz, F. Li, J. Cheng, N. Tanaka and F. J. Gonzalez, *Br. J. Pharmacol.*, 2012, **167**, 1271–1286.
23 S. Giri, J. R. Idle, C. Chen, T. Mark Zabriskie, K. W. Krausz and F. J. Gonzalez, *Chem. Res. Toxicol.*, 2006, **19**, 818–827.
24 Q. Zhao, X. M. Li, H. N. Liu, F. J. Gonzalez and F. Li, *Xenobiotica*, 2017, 1–38, just-accepted.
25 T. Kind and O. Fiehn, *BMC Bioinf.*, 2007, **8**, 105.
26 C. Xu, C. Y. T. Li and A. N. T. Kong, *Arch. Pharmacal Res.*, 2005, **28**, 249–268.
27 N. Tsunoda and H. Yoshimura, *Xenobiotica*, 1981, **11**, 23–32.
28 J. H. Lin and A. Y. H. Lu, *Pharmacol. Rev.*, 1997, **49**, 403–449.
29 J. H. Kim, H. S. Kim, T. Y. Kong, J. Y. Lee, J. Y. Kim, M. K. In and H. S. Lee, *J. Pharm. Biomed. Anal.*, 2016, **119**, 50–58.
30 J. Vrba, B. Papouskova, M. Pyszkova, M. Zatloukalova, K. Lemr, J. Ulrichova and J. Vacek, *J. Pharm. Biomed. Anal.*, 2015, **102**, 193–198.
31 K. E. Thummel and G. R. Wilkinson, *Annu. Rev. Pharmacol. Toxicol.*, 1998, **38**, 389–430.
32 X. L. Qin, X. Chen, G. P. Zhong, X. M. Fan, Y. Wang, X. P. Xue, Y. Wang, M. Huang and H. C. Bi, *Phytomedicine*, 2014, **21**, 766–772.
33 D. L. Thacker, A. Modak, P. D. Nguyen, D. A. Flockhart and Z. Desta, *Chirality*, 2011, **23**, 904–909.
34 Z. G. Lin, Z. W. Lin, Y. D. Mu and D. Yan, *Spectrochim. Acta, Part A*, 2016, **167**, 84–88.
35 C. Y. Li, L. W. Qi, P. Li, X. D. Wen, Y. F. Zhu, E. H. Liu, Z. Gong, X. L. Yang, M. T. Ren, Y. J. Li and X. X. Ge, *Rapid Commun. Mass Spectrom.*, 2009, **23**, 1977–1988.